19th Brazilian Congress of Thermal Sciences and Engineering
November 06th-10th, 2022, Bento Gonçalves - RS - Brazil

ENC-2022-0687
A THEORETICAL-EXPERIMENTAL COMPARISON FOR A FLEXIBLE PIPE ASPIRATING WATER UNDER VIV

Renato Henrique Finoteli
Wagner Antonio Defensor Filho
Renato Maia Matarazzo Orsino
Celso Pupo Pesce
Offshore Mechanics Laboratory, Escola Politécnica, University of São Paulo, Av. Professor Lúcio Martins Rodrigues, Tv. 4, n. 434, São Paulo – SP, 05508-020, Brazil
renato.finoteli@usp.br
wadfilho@usp.br
renato.orsino@gmail.com
ceppesce@usp.br

Abstract. *From an experimental campaign planned to study the dynamics of flexible pipes aspirating water under vortex-induced vibrations (VIV), carried out in the towing tank facilities at the Institute for Technological Research (IPT) - São Paulo, Brazil, this work brings a preliminary theoretical-experimental comparison. Numerical simulations, performed both with an in-house mathematical model and with a commercial software package (Orcaflex™), are performed to assess experimental scenarios. In a general agreement with the experimental results, the numerical analyses reveal that the influence of aspirating internal flow on VIV is marginal, even in a post-critical condition. The numerical models, however, were not able to fully recover the complex dynamics observed in the experiments, even though the in-house model presented better adherence to the experimental results.*

Keywords: *Vortex-Induced Vibration (VIV), Aspirating flow, Modular Modeling Methodology*

1. INTRODUCTION

Seawater intake risers (SWIRs) are long tubular flexible structures installed in floating production storage and offloading (FPSOs) platforms aiming at increasing the energy efficiency of the cooling system of their processing plant. The dynamics of this type of structure is governed by the loads associated to the internal and external flows and also by loads associated with motions imposed by the floating unity, caused by the action of free surface waves, currents and winds.

The problem of pipes conveying fluid was initially introduced by Benjamin (1961) and, since then, it has been studied by several researchers through theoretical and experimental approaches. The studies available in the specialized literature show that stability analysis is a crucial point in the dynamics of pipes aspirating fluid. An extensive literature review can be found in Païdoussis (2014). Regarding external flow effects, Vortex-Induced Vibration (VIV) is another fluid-structure interaction (FSI) phenomenon that has been extensively studied in offshore applications for being possible causes of fatigue and collapse of structures. A comprehensive review on VIV can be found in Bearman (1984).

In order to address these types of problems from a theoretical point of view, a novel modeling methodology initially introduced by Orsino (2016) for multibody systems, known as Modular Modeling Methodology (MMM), has been successfully extended to address FSI phenomena in flexible structures. Since then, a series of papers treating such problems, gradually increasing the completeness and complexity of the models, have been published. For instance, Orsino and Pesce (2018) applied the MMM to propose a non-linear planar reduced-order model of a cantilevered pipe ejecting fluid, whose linearized form was able to recover the classical results by Gregory and Païdoussis (1966). In Orsino et al. (2018), this model was extended to a 3D formulation which allowed the study of simultaneous effects of flow ejection and VIV, the latter phenomenon being modeled through a wake oscillator based on a forced van der Pol equations, which was proposed by Ogink and Metrikine (2010) for emulating the FSI due to vortex shedding in rigid cylinders. It was observed that the action of the internal flow in an ejecting pipe could either mitigate (if the internal flow velocity is below the critical value associated to a Hopf bifurcation in the model) or amplify (if above this critical value) the amplitudes of

steady state limit-cycle oscillations, when compared to pure VIV responses. More recently, Orsino et al. (2022) addressed the problem of a flexible pipe aspirating water under VIV within a 3D formulation that includes a proper account of the effects of the intake flow. The aforementioned phenomenological approach for modeling VIV effects was once again implemented.

Nevertheless, experimental data on flexible pipes either ejecting or aspirating fluid under VIV was still missing in the specialized literature. Aiming at filling this gap, a novel comprehensive experimental campaign was planned and carried out in the towing tank facilities of the Institute for Technological Research (IPT) - São Paulo, Brazil (Defensor Filho, 2022).

This paper brings part of a theoretical-experimental comparison in which numerical simulations obtained both from an in-house mathematical code, developed under the MMM, and Orcaflex™ software, are confronted with some of the experimental results obtained for the aspirating cases. The analyses revealed that, in these scenarios, the influence of the simultaneous action of internal flow is marginal when compared to the corresponding responses under pure VIV. Also, despite not being able to fully recover the complexity of the dynamic response observed in the experiments, both numerical models lead to similar qualitative results. However, the in-house model presented better adherence to the experimental results.

This paper is organized as follows: Sec. 2 presents a brief description of the experimental campaign; Sec. 3 discusses the numerical models; Sec. 4 shows a brief description of the data treatment applied to experimental and numerical models; Sec. 5 addresses a first comparison between the experimental and numerical results, discussing the effects of the aspirating internal flow on the VIV response; concluding remarks are finally drawn in Sec. 6.

2. A BRIEF DESCRIPTION OF THE EXPERIMENTS

The IPT towing tank is 240m long, 6m wide and 3.5m in depth, with maximum towing carriage speed around 4m/s. Three cantilevered flexible pipes, made of reinforced rubber hoses, clamped at an end and with a brass ballast attached to the free one, were mounted vertically, side-by-side, in a towing car as shown in Fig. 1. in order to be tested under external and internal flow excitations, both in isolated (pure) and simultaneous conditions, therefore being submitted to the same external flow velocity.

The models were designed and built with the guidance of the in-house mathematical model (Orsino et al., 2022): the length of each hose and ballast was chosen so that, under the same range of external flow velocities, each model would present VIV responses exciting primarily one of the first three natural modes of oscillation in water. Each model was named according to the achronim BH (from 'ballasted-hose' concept), followed by the number of the natural mode of vibration, $n = 1,2,3$, that was designed to be the dominant under towing excitation. Thus, models BH-1, BH-2 and BH-3 should exhibit oscillatory responses in the first, second and third natural modes of vibration, respectively, all of them planned to correspond to natural frequencies close to 1 Hz. *Root-loci* diagrams, also obtained from the linearized form of the in-house mathematical model, guided the tests, by presenting the natural periods of the experimental models in water as a function of the aspirating flow velocity. The value of internal flow velocity in which any natural mode presents a shift from stable to unstable regime was identified as a threshold of instability and labeled as a critical velocity, V_c. Values of $0.5V_c$, V_c and $2V_c$ were tested for the aspirating scenario.

The hose material is nitrile rubber with fiber reinforcement, presenting linear density of 0.56 kg/m, axial stiffness $EA = 12.5 \times 10^6$ N and bending stiffness $EI = 1.23$ Nm². The ballast is made of brass and presents a linear density of 4.15 kg/m with Young modulus $E = 105 \times 10^3$ N/mm². Both components, hose and ballast, have the same internal and external diameters, $D_i = 22$ mm and $D_e = 33$ mm, respectively, in order to minimize interferences and local effects in the external and internal flows. In the present work, only results obtained for the experimental model BH-2 are considered. The corresponding hose length is $L_h = 1595.2$ mm and the ballast length is $L_b = 110$ mm, leading to a total length of $L_m = 1705.2$ mm.

The dynamic response was measured using the Qualisys Tracking Manager™ - QTM system. It is a wireless, non-invasive optical system that tracks reflective targets (adhesive tapes) placed along the model length, measuring with high resolution their 3D cartesian coordinates, from frames obtained with high resolution (better than 0.05mm in this case, Salles and Pesce, 2019) and high-speed underwater cameras. Model BH-1 was instrumented with 8 tapes, models BH-2 and BH-3 with 18 and 32 tapes, respectively. The natural frequency of interest for the experimental model BH-2, related to the second vibration mode, was assessed by dynamic characterization in air and is $f_{2y} = 1.18$ Hz. Further details concerning this experimental campaign can be found in Defensor Filho (2022) and Pesce et al. (2021).

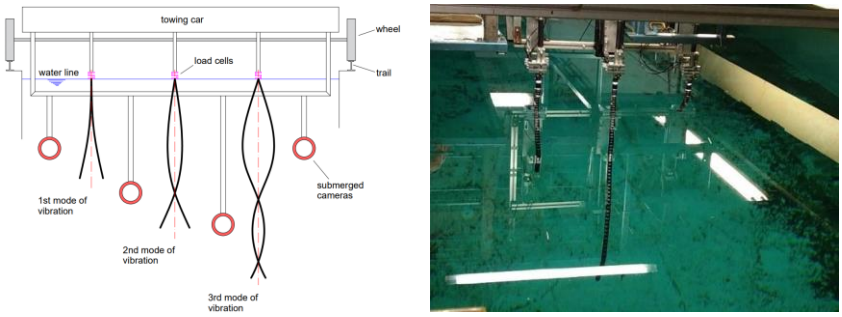

Figure 1: (Left) Scheme of the three flexible models arrangement exhibiting oscillations in the 1st, 2nd and 3rd modes of vibration (from left to right); extracted from Pesce et al. (2021). (Right) Experimental models in their actual assembly in the towing tank (from left to right: BH-2, BH-3 and BH-1).

3. NUMERICAL MODELS

One objective of the present work is to assess the dynamic response of two numerical models developed with the same parameters and dimensions of the experimental model BH-2 and submitted to the same excitation scenarios. The first of them is an in-house mathematical model and the second one was implemented in Orcaflex™, a well-recognized commercial software for studying riser dynamics. Another objective is to promote a comparison between the experimental responses and the ones obtained by the numerical models in the same scenarios.

3.1 The in-house model via MMM

The in-house mathematical model is an extended version of the one introduced by Orsino et al. (2022), constituted by a single homogeneous flexible pipe. The version used in the present work includes a rigid ballast segment attached to the flexible pipe's free end. The FSI phenomena are modeled by the same strategies for both segments, the flexible and the rigid ones. The derivation of the model accounted the following hypotheses: the pipe's material is inextensible, homogeneous and satisfies the hypotheses of linear elasticity (large displacements admissible); the system is a slender cantilevered cylinder, vertically mounted and immersed in water; the external flow's profile velocity is assumed to be uniform, constant and horizontal; aspirating internal flow and external flow are kept at a constant rate during the tests; internal flow is modeled as a plug flow, except at the inlet sector where the velocity profile is corrected by a shaping factor χ (estimated from a CFD analysis performed with the commercial software STAR-CCM+), modeling the distortion of the actual flow profile at the inlet with respect to a uniform profile; VIV is modeled according to the phenomenological model proposed by Ogink and Metrikine (2010). To derive the complete model, the authors used the extended form of Hamilton's principle for non-material volumes (Casetta and Pesce, 2013):

$$\delta \int_{\tau_1}^{\tau_2} (L + \mathcal{R})\, d\tau + \int_{\tau_1}^{\tau_2} \delta W d\tau = 0 \tag{1}$$

In this equation, L denotes the Lagrangian of the system, modeling effects due to inertia, flexural stiffness and gravity (including buoyancy); $\mathcal{R}$ denotes the Rayleighian structural damping; δW denotes a sum of virtual work parcels modeling effects related to external hydrodynamic forces, added mass, lift and drag (due to the pipe interaction with external flow), and to the flux of momentum (due to the flow in the inlet section of the pipe). Let l be the total length of the flexible pipe and m_d, the total mass of water displaced in external media due the presence of the pipe, so that the scales adopted for length, time and mass are given by l, $\sqrt{m_d l^3/EI}$ and m_d, respectively.

Define a coordinate system fixed to an inertial reference frame $N = (O, \hat{\boldsymbol{n}}_1, \hat{\boldsymbol{n}}_2, \hat{\boldsymbol{n}}_3)$, where the origin of this system is given by the center O, which represents the center of the outlet (clamped) section, see Fig. 2. The non-dimensional arc-length coordinate ξ is measured along the centerline of the pipe from the clamped end, where $\xi = 0$, to the free end of the flexible pipe, where $\xi = 1$. The center of each cross section along the arc-length is denoted by C_ξ. Let $\vec{\boldsymbol{r}}$ be the non-dimensional position vector of a given point from the center O to C_ξ. The partial derivatives of $\vec{\boldsymbol{r}}$ with respect to the non-dimensional arc-length coordinate ξ and to the non-dimensional time τ are given by prime and dot notation, respectively.

Let $\vec{\boldsymbol{u}}_\xi$ be a horizontal vector that defines the shape of this free-stream profile, which in this work is simply given by $\hat{\boldsymbol{n}}_1$. The magnitude of the external and internal flows are given by u and v, respectively. For each cross section of the pipe, define a local orthonormal basis $(\hat{\boldsymbol{d}}_\xi, \hat{\boldsymbol{l}}_\xi, \hat{\boldsymbol{t}}_\xi)$ to represent the system S_ξ, such that $\hat{\boldsymbol{t}}_\xi = \vec{\boldsymbol{r}}'$ and $\hat{\boldsymbol{l}}_\xi$ is defined as a unit vector orthogonal to $\vec{\boldsymbol{u}}_\xi$. The components of the position vector of the flexible pipe can be expressed in terms either of the generalized coordinates r_k $(k = 1,2,3)$ or of the quasi-coordinates x_k $(k = 1,2,3)$. Defining μ_p and μ_i as the linear mass densities of the pipe itself and of the fluid inside the pipe, respectively, and $\gamma = gl^2 m_d/EI$, the Lagrangian, Rayleigh damping and virtual work of the flexible pipe can be expressed by:

$$L_p = \frac{1}{2}\int_0^1 \left[(\mu_p + \mu_i)(\dot{\vec{r}}\cdot\dot{\vec{r}}) - 2\mu_i\, v(\dot{\vec{r}}\cdot\vec{r}') + \mu_i v^2(\vec{r}'\cdot\vec{r}') - \vec{r}''\cdot\vec{r}'' + 2\gamma(\mu_p + \mu_i - 1)\vec{r}\cdot\hat{\boldsymbol{n}}_3\right]d\xi \tag{2}$$

$$\mathcal{R}_p = \frac{1}{2}\int_0^1 \beta_p\,(\dot{\vec{r}}\cdot\dot{\vec{r}})d\xi \tag{3}$$

$$\delta W_p = -\int_0^1 \ddot{\vec{x}}\cdot\left(\mu_{a,1}\hat{\boldsymbol{d}}_\xi\hat{\boldsymbol{d}}_\xi + \mu_{a,2}\hat{\boldsymbol{l}}_\xi\hat{\boldsymbol{l}}_\xi + \mu_{a,3}\hat{\boldsymbol{t}}_\xi\hat{\boldsymbol{t}}_\xi\right)\cdot\delta\vec{\boldsymbol{x}}d\xi + \int_0^1 \frac{2u^2}{\pi d_e}\left(c_1\hat{\boldsymbol{d}}_\xi + c_2\hat{\boldsymbol{l}}_\xi\right)\cdot\delta\vec{\boldsymbol{x}}d\xi \tag{4}$$

In these expressions, β_p is a nondimensional constant of proportional damping of the flexible pipe, $\mu_{a,k}$ $(k = 1,2,3)$ are the nondimensional added mass coefficients along the directions $(\hat{\boldsymbol{d}}_\xi, \hat{\boldsymbol{l}}_\xi, \hat{\boldsymbol{t}}_\xi)$, d_e is the nondimensional external diameter and c_n $(n = 1,2)$ represent the hydrodynamic force coefficients expressed in the local system of coordinates S_ξ. The same can be applied to the rigid ballast segment:

$$L_b = \frac{1}{2}\int_1^{1+L_b} \left[(\mu_b + \mu_i)(\dot{\overrightarrow{\boldsymbol{r_b}}}\cdot\dot{\overrightarrow{\boldsymbol{r_b}}}) - 2\mu_i\, v(\dot{\overrightarrow{\boldsymbol{r_b}}}\cdot\overrightarrow{\boldsymbol{r_b}}') + \mu_i v^2(\overrightarrow{\boldsymbol{r_b}}'\cdot\overrightarrow{\boldsymbol{r_b}}') + 2\gamma(\mu_b + \mu_i - 1)\overrightarrow{\boldsymbol{r_b}}\cdot\hat{\boldsymbol{n}}_3\right]d\xi \tag{5}$$

$$\mathcal{R}_b = \frac{1}{2}\int_1^{1+L_b} \beta_b\,(\dot{\overrightarrow{\boldsymbol{r_b}}}\cdot\dot{\overrightarrow{\boldsymbol{r_b}}})d\xi \tag{6}$$

$$\begin{aligned}\delta W_p = -\int_1^{1+L_b} \ddot{\vec{\boldsymbol{x}}}_b\cdot\left(\mu_{b\,a,1}\hat{\boldsymbol{d}}_\xi\hat{\boldsymbol{d}}_\xi + \mu_{b\,a,2}\hat{\boldsymbol{l}}_\xi\hat{\boldsymbol{l}}_\xi + \mu_{b\,a,3}\hat{\boldsymbol{t}}_\xi\hat{\boldsymbol{t}}_\xi\right)\cdot\delta\vec{\boldsymbol{x}}_{\boldsymbol{b}}d\xi + \int_1^{1+L_b}\frac{2u^2}{\pi d_{b_e}}\left(c_{1_b}\hat{\boldsymbol{d}}_\xi + c_{2_b}\hat{\boldsymbol{l}}_\xi\right)\cdot\delta\vec{\boldsymbol{x}}_{\boldsymbol{b}}d\xi \\ + \left[\mu_i v\left(\dot{\overrightarrow{\boldsymbol{r_b}}} - \chi v\overrightarrow{\boldsymbol{r_b}}'\right)\cdot\delta\vec{\boldsymbol{x}}_{\boldsymbol{b}}\right]\Big|_{\xi=1+L_b}\end{aligned} \tag{7}$$

Equations (5)- (7) are similar to Eqs. (2)-(4), but now the present terms refer to the rigid ballast segment (indicated by the subscript b) and there is also the flux of momentum due to the flow in the inlet section of the ballast. Thus, the total parts of the Lagrangian, Rayleigh damping and virtual work of the system are given by:

$$L = L_p + L_p,\ \mathcal{R} = \mathcal{R}_p + \mathcal{R}_b,\ \text{and}\ \delta W = \delta W_p + \delta W_b \tag{8}$$

In the scope of the MMM, the equations of motion for that would be obtained if the constraints of the model were relaxed are obtained by applying Eqs. (2)-(7) in Eq. (8) and then substituting in Eq. (1). The structural constraint equations to be satisfied for the "relaxed model" to be compatible with the original model are given by:

$$\begin{gathered}\vec{\boldsymbol{r}}' = \hat{\boldsymbol{t}}_\xi, \qquad \hat{\boldsymbol{l}}_\xi\cdot\vec{\boldsymbol{u}}_\xi = 0, \qquad (\ddot{r}_1, \ddot{r}_2, \ddot{r}_3)^T = \boldsymbol{R}_\xi(\ddot{x}_1, \ddot{x}_2, \ddot{x}_3)^T, \\ (\overrightarrow{\boldsymbol{r_b}} - \vec{\boldsymbol{r}})|_{\xi=1} = \vec{0},\ \text{and}\ (\overrightarrow{\boldsymbol{r_b}}' - \vec{\boldsymbol{r}}')|_{\xi=1} = \vec{0}\end{gathered} \tag{9}$$

In this equation, $\boldsymbol{R}_\xi$ represents the rotation-matrix between the coordinate systems S_ξ and N. The constraint equations referring to the hydrodynamic force coefficients are given by:

$$\left(u + \dot{w}_\xi\right)^2 = \left(\left(u\vec{\boldsymbol{u}}_\xi - \dot{\vec{\boldsymbol{r}}}\right)\cdot\hat{\boldsymbol{d}}_\xi\right)^2 + \left(\dot{\vec{\boldsymbol{r}}}\cdot\hat{\boldsymbol{l}}_\xi\right)^2 \tag{10}$$

$$\dot{c}_1 = \frac{u+\dot{w}_\xi}{u^2}\left[\overline{C}_D^0\left(u\vec{\boldsymbol{u}}_\xi - \dot{\vec{\boldsymbol{r}}}\right)\cdot\hat{\boldsymbol{d}}_\xi + \frac{q_\xi}{\hat{q}}\hat{C}_L^0\dot{\vec{\boldsymbol{r}}}\cdot\hat{\boldsymbol{l}}_\xi\right],\ \text{and}\ \dot{c}_2 = \frac{u+\dot{w}_\xi}{u^2}\left[\frac{q_\xi}{\hat{q}}\hat{C}_L^0\left(u\vec{\boldsymbol{u}}_\xi - \dot{\vec{\boldsymbol{r}}}\right)\cdot\hat{\boldsymbol{d}}_\xi - \overline{C}_D^0\dot{\vec{\boldsymbol{r}}}\cdot\hat{\boldsymbol{l}}_\xi\right] \tag{11}$$

In these equations, $\dot{w}$ is a perturbation in the relative velocity with respect to the value it has in the static equilibrium configuration, $\overline{C}_D^0$ is the mean drag coefficient, $\hat{C}_L^0$ is the amplitude of the lift coefficient of a stationary rigid cylinder and $\hat{q} = 2$. The wake variables q_ξ are defined locally in each cross-section, following the phenomenological model proposed by Ogink and Metrikine (2010). The rigid ballast segment has similar constraint equations for the hydrodynamic force coefficients.

Let $\boldsymbol{q}$ be the generalized coordinates vector. Writing down the "relaxed model" in the matrix form $\boldsymbol{M}\ddot{\boldsymbol{q}} = \boldsymbol{f}$ and the constraint equations in the form $\boldsymbol{A}\ddot{\boldsymbol{q}} = \boldsymbol{b}$, and computing a matrix $\boldsymbol{S}$ whose image describes the kernel of $\boldsymbol{A}$, the reduced-order model of the original system is given by:

$$\begin{bmatrix} \boldsymbol{S^T M} \\ \boldsymbol{A} \end{bmatrix} \ddot{\boldsymbol{q}} = \begin{bmatrix} \boldsymbol{S^T f} \\ \boldsymbol{b} \end{bmatrix} \tag{12}$$

Again, for the complete description of the in-house mathematical model, the reader is referred to Orsino et al. (2022), Pesce et al. (2022) and Finoteli (2022).

3.2 The Orcaflex™ model

The model in Orcaflex™ is divided in two-line segments modeled as a homogeneous pipe, one to represent the flexible pipe and a second to represent the rigid ballast. The external flow profile is considered uniform in magnitude and direction, with the FSI associated with the external flow emulated through the phenomenological model of Iwan and Blevins (1974), using the default hydrodynamic parameters presented in the Orcaflex™, i.e., $a_0 = 0.48$, $a_1 = 0.44$, $a_2 = 0.20$, $a_3 = 0.00$, $a_4 = 0.38$ and $St = 0.20$.

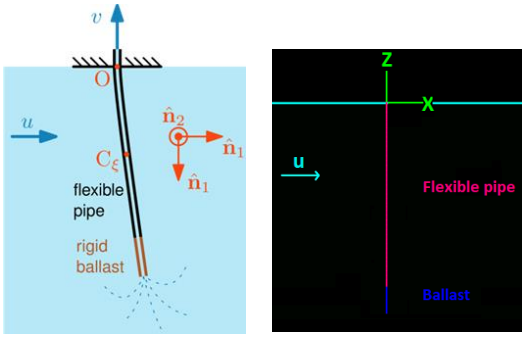

Figure 2. Representation of the in-house and Orcaflex™ numerical models. Extracted from Pesce et al. (2022).

4. DATA TREATMENT

The data obtained from the simulations with the numerical models in the in-house and Orcaflex™ codes were submitted to the same post-processing analyses adopted for the experiments. Time series of Cartesian coordinates were obtained for the same 18 vertical positions as in the experimental model BH-2. The applied treatment brings two types of results: standard information along the model's length and modal responses. The standard information presents the targets' trajectory projections, their mean values, amplitude standard deviation and the amplitude spectrum obtained via the Fast Fourier Transform (FFT) algorithm. The modal results were obtained by modal decomposition both in streamwise and crosswise directions using Galerkin's method. The projection functions are compatible with the boundary conditions of the model and were obtained from the in-house mathematical model as the modal shapes for natural oscillations around the equilibrium positions considering the nominal external flow velocities adopted in the experimental tests. The modal analyses present the dimensionless amplitude (per unit of external diameter of the pipe) contribution up to the 5^{th} natural mode of vibration with the respective dimensionless dominant frequencies for each reduced-velocity tested. Once again, for further details concerning the experimental data treatment, the reader is referred to Defensor Filho (2022) and to Pesce et al. (2021).

5. RESULTS COMPARISON: EXPERIMENTAL VS IN-HOUSE MODEL VS ORCAFLEX™

This section compares the experimental results of the model BH-2 with the corresponding numerical ones obtained both from in-house and Orcaflex™ models. Two types of scenarios are discussed: pure towing and towing with aspirating internal flow in post-critical condition, with $2V_c$. In the pure towing scenarios, tests were performed for 20 different values of external flow velocity, while for the cases of towing and aspirating internal flow with $2V_c$, only five values of external flow velocity were tested. First, the dimensionless modal amplitude contributions are presented, $A^*_{nx} = A_{nx}/D$ and $A^*_{ny} = A_{ny}/D$, where n stands for the vibration mode n, with the respective dimensionless dominant frequencies, $F^*_{nx} = F_{nx}/f_{2y}$ and $F^*_{ny} = F_{ny}/f_{2y}$, where F_n stands for the dominant frequency in the modal amplitude series, f_{2x} and f_{2y} are the natural frequencies corresponding to the second vibration mode in the streamwise and crosswise directions to the incident flow, respectively. After that, the results for one specific towing velocity are depicted as an illustrative case in which the amplitudes of response along the length are visible in more detail. Table 1 shows a comparison between the natural frequencies of interest determined from the experimental and numerical models with the selected reduced-velocities. It is possible to observe that the natural frequency of interest of the in-house model was the one that presents the smallest difference compared to that measured experimentally.

Table 1 - Comparison between the natural frequencies and the selected reduced-velocity between experimental model BH-2, Orcaflex™ model and in-house model.

Parameter	Experimental	Orcaflex™	In-house
f_{2y} $[Hz]$	1.18	1.11	1.12
Δ [%]	-	5.7%	4.9%
$U_{2y}^* = U/f_{2y}D$, with $U = 0.252$ m/s	6.48	6.88	6.82

5.1 VIV UNDER TOWING

In each chart in Figure 3 the dimensionless modal amplitude contributions are presented, $A_{n\,x,y}^*$, and the respective dimensionless dominant frequencies, $F_{n\,x,y}^*$, as function of reduced-velocity, U_{2y}^*, corresponding to natural modes, n, from 1 to 5. Figure 3a presents the response of experimental model BH-2 while Figs. 3b and 3c show the corresponding responses for Orcaflex™ and in-house simulations, respectively. Charts on the left depict the responses in the streamwise direction while the ones in the right show the responses in the crosswise direction.

The experimental response in the crosswise direction shows the second natural mode dominating the response in the reduced-velocity range $5 < U_{2y}^* < 9$ with amplitude contributions up to $A_{2y}^* = 1.2$. Such a response was expected, since the model was designed to have a dominant oscillatory response in the second mode. The first mode presents amplitude contributions up to $A_{1y}^* = 0.9$, in the same reduced-velocity range, synchronized with the second mode resonance, since all modes present dominant frequencies of oscillation $F_{ny}^* = 1$. The resonance of the first crosswise natural mode happens in the initial values of reduced-velocity, $1.5 < U_{2y}^* < 3$. The respective dominant crosswise frequencies, $F_{n\,y}^*$, are well behaved up to $U_{2y}^* = 9$, from where they become scattered. In the streamwise direction, strong resonance occurs practically in the same range of reduced-velocity, $5 < U_{2y}^* < 9$, with the first and second modes presenting almost the same amplitude contribution, $A_{1,2\,x}^* \sim 0.3$, with the respective dominant frequencies values close to $F_{1,2\,x}^* \sim 2$.

The Orcaflex™ simulation presented, in the crosswise direction, the resonance region in the range $4 < U_{2y}^* < 7$, with modal amplitude contributions from the first mode significantly exceeding the experimental ones. Contributions from the third natural mode appeared in $U_{2y}^* > 10$, which are not observed in the experimental response. The respective crosswise dominant frequencies increased in a well-behaved manner; however, exceeding the experimental values. In the streamwise direction, modes' contributions are weak, the respective dominant frequencies presenting, once more, higher values than the experimental ones.

Regarding the in-house code, the resonance regions in the streamwise and crosswise directions are also left-shifted to the reduced-velocity range, $4 < U_{2y}^* < 7$, when compared to the experimental results. However, the modal amplitude contributions and the respective dominant frequencies are much more similar to the experimental values, if compared to those from Orcaflex™.

Figure 4 presents the trajectories projections, standard deviation and the amplitude spectra along the cylinder's length, for one specific flow velocity. As before, Fig. 4a presents the response of the experimental model BH-2, while Figs. 4b and 4c show the responses from Orcaflex™ and from the in-house models, respectively. The chosen flow velocity is $U = 0.25$ m/s, corresponding to the reduced-velocity $U_{2y}^* = 6.48$ for the experimental model BH-2, $U_{2y}^* = 6.87$ and $U_{2y}^* = 6.81$ for the Orcaflex™ and in-house numerical models, respectively. The difference in the U_{2y}^* is due to the differences among the values of natural frequencies shown in Table 1. The trajectory projections show a clear second natural mode shape for all three models in the crosswise direction, with the numerical simulations presenting smaller amplitudes. Also, the amplitude spectra for the experimental and the in-house models present the frequencies closer to $f_y^* \approx 1.0$, while in Orcaflex™ simulation is almost $f_y^* \approx 4.0$. In streamwise direction, the second natural mode shape is visible for the experiment and both simulations, although with the latter presenting insignificant contributions in amplitude. Subharmonics can be seen in the crosswise direction in the experimental and Orcaflex™ responses. Nevertheless, frequencies in the in-house simulations are more adherent to the experimental ones, in contrast to the higher values presented by the Orcaflex™ simulation. In a general way, it is clear that the in-house model presented a response that was quantitatively and qualitatively closer to the experimental results than the present Orcaflex™ model.

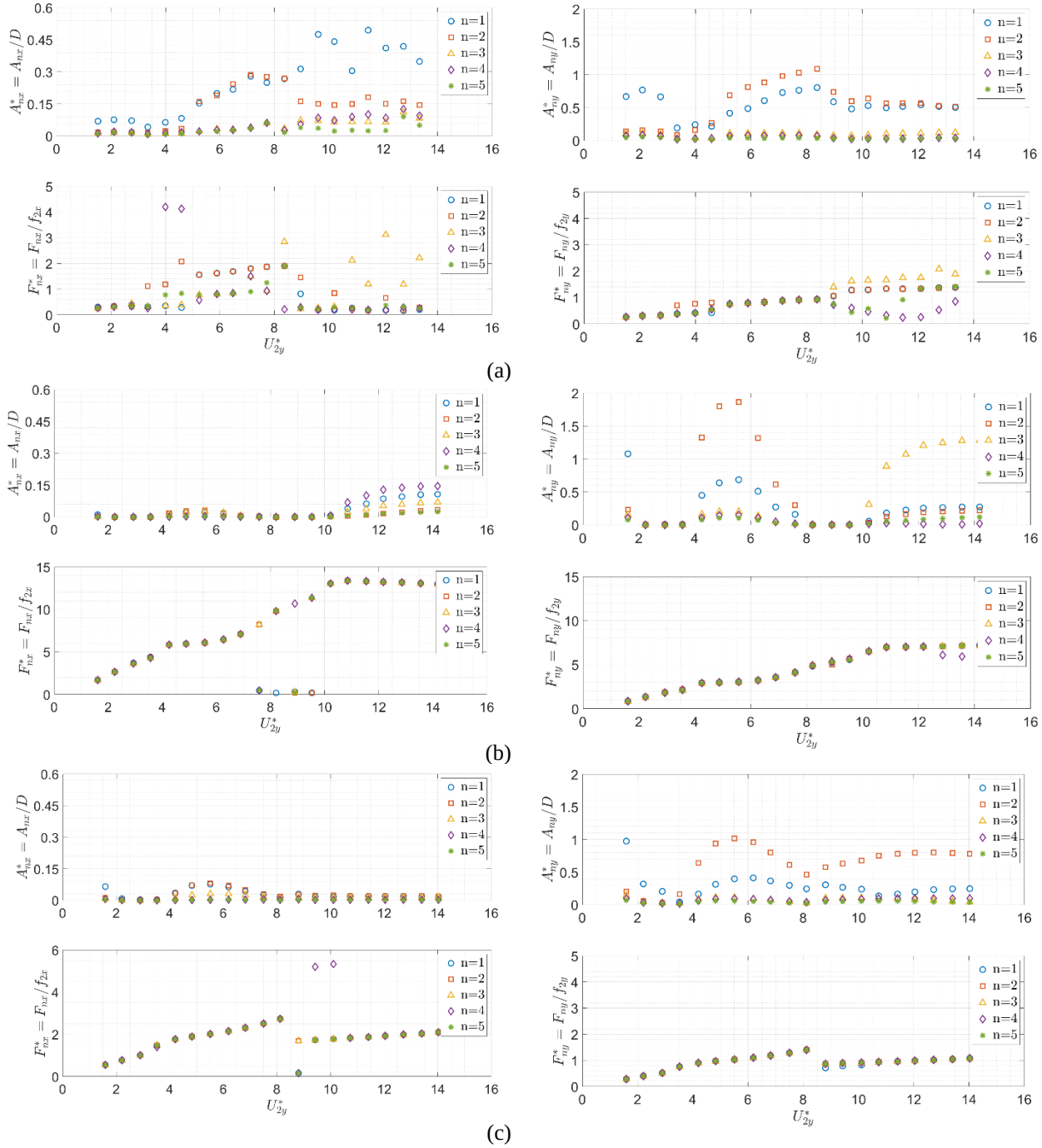

Figure 3. Dimensionless modal amplitude contributions, $A^*_{n\,x,y}$, and respective dimensionless dominant frequencies, $F^*_{n\,x,y}$, as function of reduced-velocity U^*_{2y}; n from 1 to 5. (a), (b) and (c): Experimental, Orcaflex™ and in-house, respectively. (Left and right) Streamwise and crosswise directions, respectively.

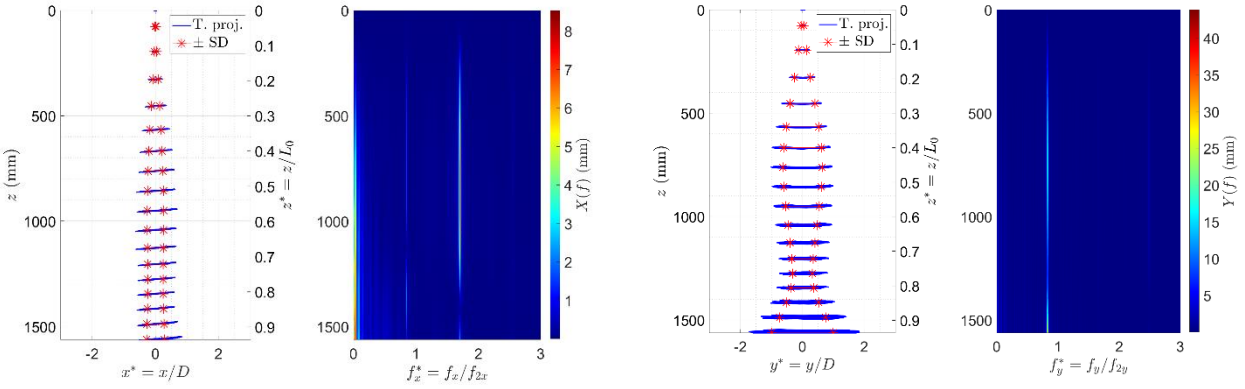

(a)

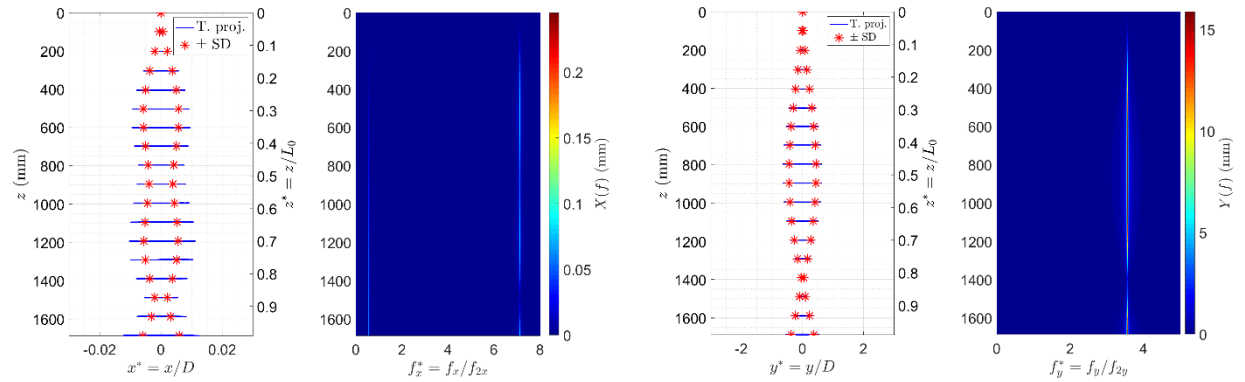

(b)

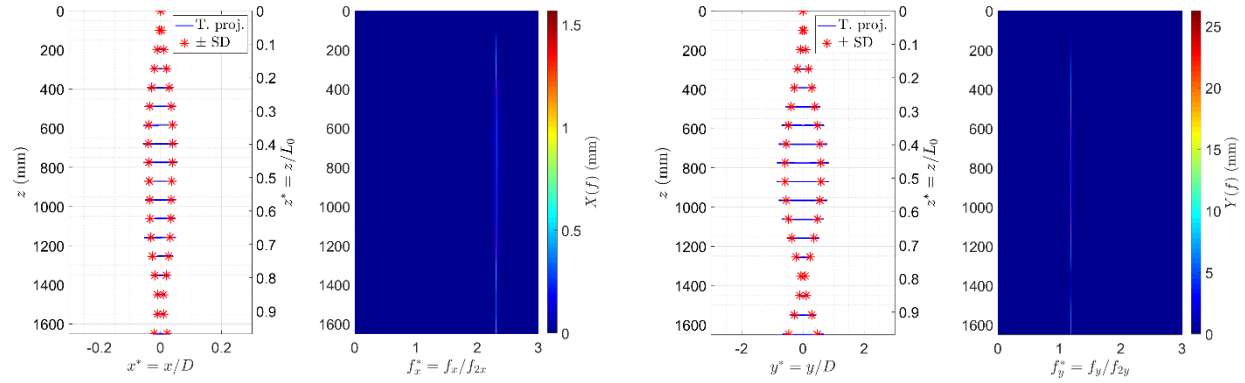

(c)

Figure 4. Trajectory projections around time-average position and amplitude spectra as function of the dimensionless frequency, for each target. (a), (b) and (c): Experimental, Orcaflex™ and in-house, respectively. (Left and right) Streamwise and crosswise directions, respectively.

5.2 TOWING AND ASPIRATING INTERNAL FLOW WITH $2V_c$

In this subsection the combined cases of towing and water aspiration with the internal flow velocity twice the critical value, $2V_c$ are presented. The results in Figs. 5 and 6 correspond analogously to the ones presented in Figs. 3 and 4, discussed in the last section. In general, the aspirating internal flow with $2V_c$ caused a marginal interference in the external flow effects with just a small decrease in the modal amplitudes and in the respective dominant frequencies, when compared to the pure towing case. The chosen flow velocity for detailing the response along the cylinder's length is the same as before, $U = 0.25$ m/s, corresponding to $U_{2y}^* = 6.48$ for the experimental model BH-2, $U_{2y}^* = 6.87$ and $U_{2y}^* = 6.81$ for the Orcaflex™ and in-house numerical models, respectively.

Figure 5 shows that the modal amplitude contributions in both, streamwise and crosswise directions, are slightly smaller than in the case of pure towing, with the respective dominant frequencies less sparse. The trajectory projections and amplitude spectra in Fig. 6 continue to present a consistent second natural mode shape for both directions. Once again, subharmonics are present in the experimental and Orcaflex™ amplitude spectra, in the streamwise direction. It is

worth highlighting the large difference regarding modal dominant frequencies values in Orcaflex™ model, from the case of pure towing to the present one (compare Figs. 5b and 3b on the left as well as Figs. 6b and 4b). In the present case, under aspirating flow, Orcaflex™ results are much closer to that presented by the experimental model BH-2. Once again, it can be stated that the in-house mathematical model response was more adherent to the experimental results than the response presented by the present Orcaflex™ simulations.

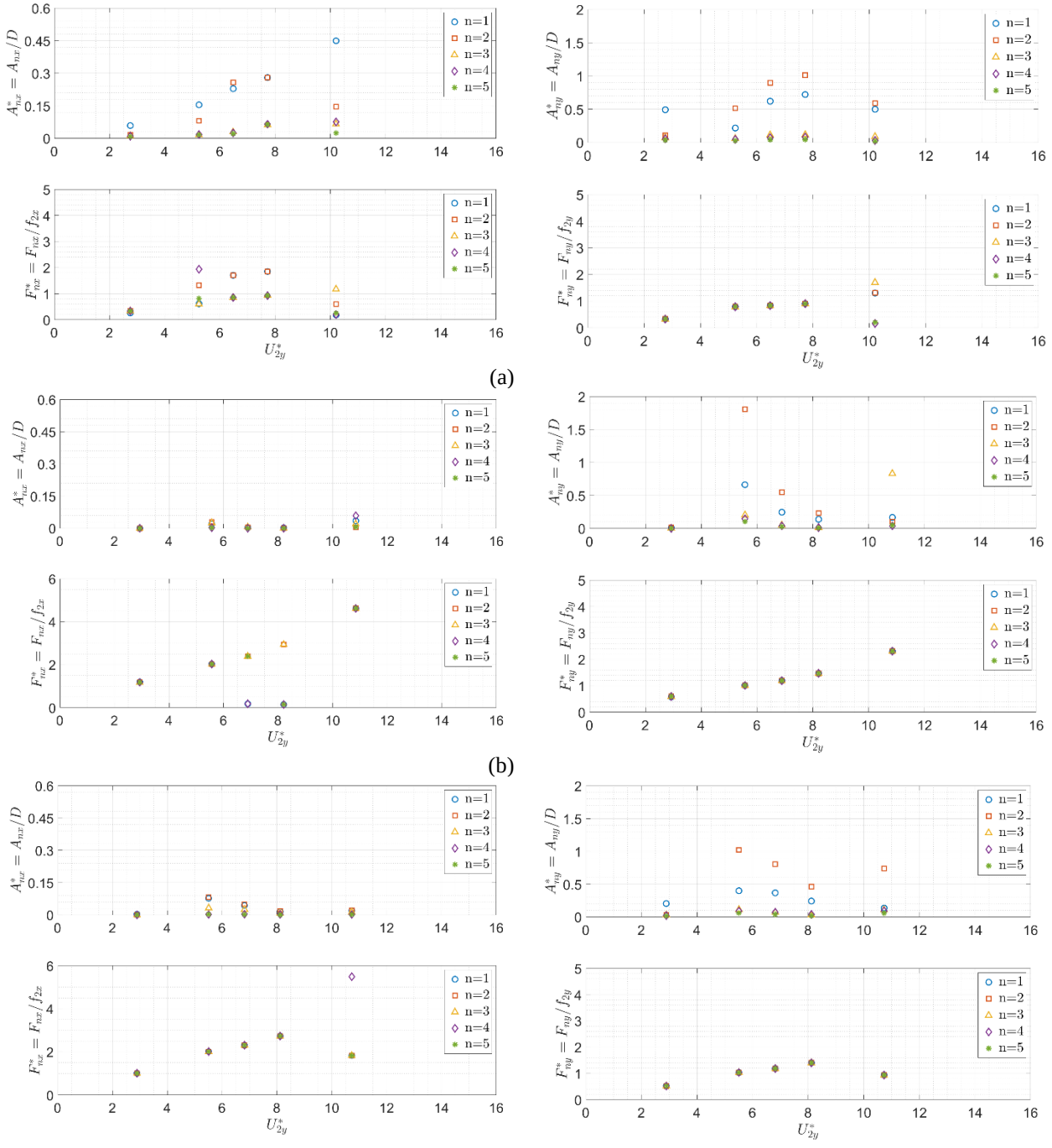

Figure 5. Dimensionless modal amplitude contributions, $A^*_{n\,x,y}$, and respective dimensionless dominant frequencies, $F^*_{n\,x,y}$, as function of reduced-velocity U^*_{2y}; n from 1 to 5. (a), (b) and (c): Experimental, Orcaflex™ and In-house, respectively. (Left and right) Streamwise and crosswise directions, respectively.

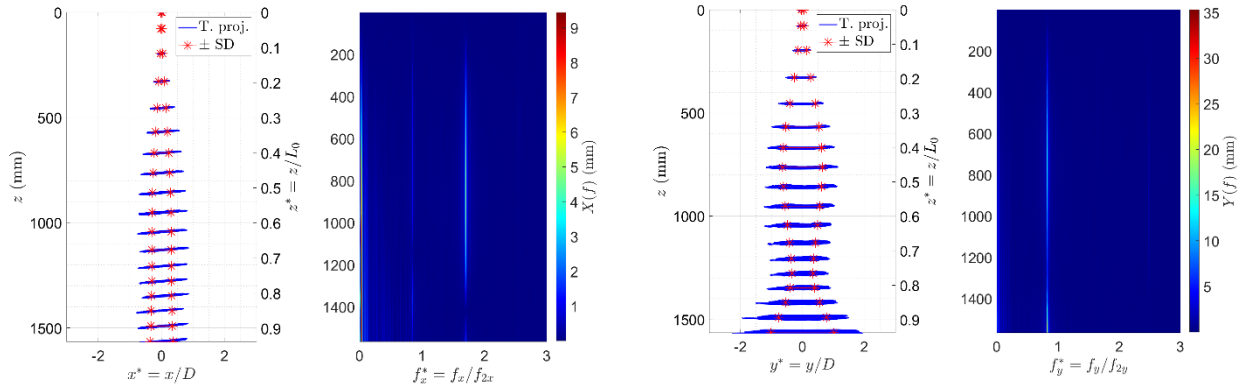

(a)

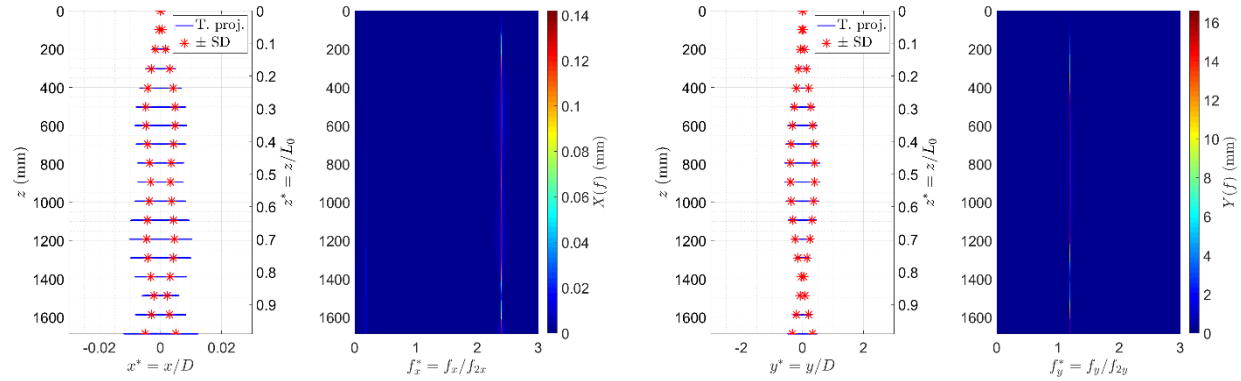

(b)

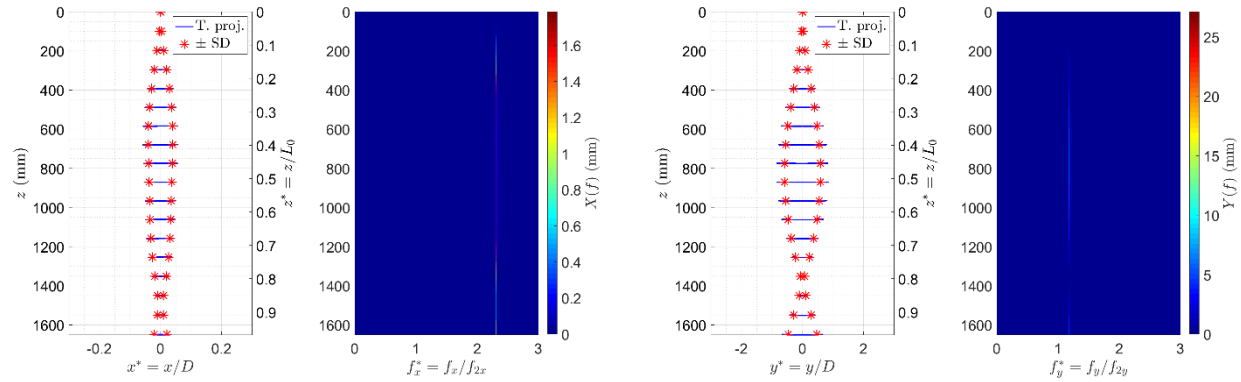

(c)

Figure 6. Trajectory projections around time-average position and amplitude spectra as function of the dimensionless frequency, for each target. (a), (b) and (c): Experimental, Orcaflex™ and in-house, respectively. (Left and right) Streamwise and crosswise directions, respectively.

6. CONCLUSION

This paper presented a numerical-experimental comparison of a cantilevered flexible pipe subjected to VIV and internal flow effects in post-critical aspirating condition. Two numerical models were developed, reproducing the same parameters of the experiments and were simulated in the same test conditions. The first was developed in the well-recognized Orcaflex™ software and the second one is an in-house mathematical model. The same analysis procedures adopted for the experimental data were applied in the numerical ones.

The results were presented as modal amplitude contributions and their respective dominant oscillation frequencies, as function of reduced-velocity. Trajectory projections and amplitude spectra taken along the models' length, for a specific value of reduced-velocity were also illustrated, for a chosen scenario.

It was observed that the region of higher excitations in the numerical models was dislocated to smaller values of reduced-velocity when compared to the experimental response, although the in-house model presented amplitudes and frequencies quantitatively more adherent to the experimental response than the Orcaflex™ model. Such a shift induces

the need to a further calibration in some of the parameters of phenomenological model used in the in-house model. Both numerical models presented dominant frequencies with values closer to the frequency of the mode of resonance when compared to the experimental frequencies, especially in the streamwise direction. This characteristic is expected since the dynamics observed in the experiments is much richer than the one captured by the models.

The experimental results showed that the aspirating internal flow in the post-critical dynamic regime (with twice the nominal critical velocity) caused minor effects on the VIV. Indeed, the aspirating flow slightly diminished the modal amplitude contributions and turned the respective dominant frequencies closer to the frequency of the mode in resonance, possibly by mitigating low frequency contents, especially in the streamwise direction. The numerical models presented the same amplitude mitigation and frequency concentration around the resonant mode's response caused by the aspirating internal flow. However, it is worth mentioning how the values of the dominant frequencies in the Orcaflex™ model were much diminished in comparison to the practically unaltered in-house model response.

In conclusion, the numerical models did not fully recover the dynamics presented in the experiments, although, the in-house model presented results quantitatively and qualitatively more adherent to experimental ones, than those presented by the Orcaflex™ model.

7. ACKNOWLEDGEMENTS

The authors gratefully acknowledge Shell Brasil for sponsoring this research work and ANP (Brazil's National Oil, Natural Gas and Biofuels Agency) for the strategic support provided through the R&D levy regulation. The authors are grateful to Professor Dr. Guilherme R. Franzini, Eng. Guilherme Vernizzi and Eng. Vitor Schwenck for encouraging discussions and for the precious help on the construction of a robust data analysis methodology. Special thanks to Eng. Cristiano Emilio Justiniano, Prof. Dr. Gustavo Assi, Dr. Pedro C. de Mello and the IPT towing tank technical staff, especially to Dr. André Kogishi, for their assistance during the experimental campaign. The first and fourth authors acknowledge research grants from CAPES and from CNPq, n. 88887.464590/2019-00 and n. 308230/2018-3, respectively. The second author acknowledges a PPGEN - Graduate Program in Ocean and Naval Engineering CAPES-PhD scholarship and a FUSP DR-C scholarship project nº 3456.

8. REFERENCES

Bearman, P.W., 1984. "Vortex shedding from oscillating bluff bodies". *Annu. Rev. Fluid Mech*, Vol. 16, pp. 195-222.

Benjamin, T.B., 1961. "Dynamics of a system of articulated pipes conveying fluid-I. Theory". *Proceedings of the Royal Society of London. Series A. Mathematical and Physical Sciences,* Vol. 261, No. 1307, pp. 457-486.

Casetta, L., and Pesce, C.P., 2013. "The generalized Hamilton's principle for a non-material volume". Acta Mechanica, Vol. 224, No. 4, pp. 919-924.

Defensor Filho, W.A., 2022. "*New Experiments with Flexible Cantilevered Pipes in Water: Aspirating Pipes Under VIV and Discharging Pipes in Post Critical Dynamic Regime".* Ph.D. thesis, Universidade de São Paulo, São Paulo, Brasil.

Finoteli, R.H., 2022. "*Comparação teórico-experimental de um tubo flexível aspirando água e sujeito ao fenômeno de Vibração Induzida por Vórtices (VIV)"*. Msc Dissertation (in Portuguese), Universidade de São Paulo, São Paulo, Brasil.

Gregory, R.W. and Païdoussis, M.P., 1966. "Unstable oscillation of tubular cantilevers conveying fluid. I. Theory". *Proceedings of the Royal Society of London. Series A. Mathematical and Physical Sciences*, v. 293, n. 1435, p. 528-542, 1966.

Iwan, W.D and Blevins, R.D., 1974. "A model for vortex induced oscillation of structures". *Journal of Applied Mechanics,* Vol. 41, pp. 581-586.

Ogink, R.H.M. and Metrikine, A.V., 2010. "A wake oscillator with frequency dependent coupling for the modeling of vortex-induced vibration". *Journal of Sound and Vibration, Elsevier,* Vol. 329, No. 26, pp. 5452-5473.

Orsino, R.M.M., 2016. *A contribution on modeling methodologies for multibody systems*. Ph.D. thesis, Universidade de São Paulo, São Paulo, Brasil.

Orsino, R.M.M. and Pesce, C.P., 2018. "Reduced order modeling of a cantilevered pipe conveying fluid applying a modular methodology". *International Journal of Non-Linear Mechanics,* Vol. 103, pp. 1-11.

Orsino, R.M.M., Pesce, C.P. and Franzini, G.R., 2018. "A 3D non-linear reduced order model for a cantilevered pipe conveying fluid under VIV." *Proc. 9th International Symposium on Fluid-Structure Interactions, Flow-Sound Interactions, Flow-Induced Vibration & Noise, FIV 2018,* Vol. 11.

Orsino, R.M.M., Pesce, C.P., Toni, F.G., Defensor Filho, W.A. and Franzini, G.R, 2022. "A 3D Nonlinear Reduced-Order Model of a Cantilevered Aspirating Pipe Under VIV". *In: Advances in Nonlinear Dynamics.* Springer, Cham, pp. 107-117.

Païdoussis, M.P., 2014. *Fluid-Structure Interactions: Slender Structures and Axial Flow.* Vol. 1, Academic Press, Elsevier Science, London.

Pesce, C.P., Franzini, G.R., Orsino, R.M.M., Assi, G.R.S., Defensor Filho, W.A., Vernizzi, G.L., Tomin, D., Maciel, V.S. and Finoteli, R.H., 2021. TR-HT-02.1: Small scale fundamental experimental tests at IPT towing tank: Experimental analysis of flexible pipes aspirating water. *Tech. rep. Restricted access.* Offshore Mechanics Laboratory - Escola Politécnica da Universidade de São Paulo.

Pesce, C.P., Franzini, G.R., Orsino, R.M.M., Assi, G.R.S., Defensor Filho, W.A., Vernizzi, G.L., Tomin, D., Maciel, V.S. and Finoteli, R.H., 2022. TR-HT-04.0: Experimental-theoretical correlation of flexible pipes aspirating water. *Tech. rep. Restricted access.* Offshore Mechanics Laboratory - Escola Politécnica da Universidade de São Paulo.

Salles, R. and Pesce, C.P., 2019. "Experimental assessments of the added mass of flexible cylinders in water: the role of modal shape representation. In: Fleury, A., Rade, D., Kurka, P. (eds) *Proceedings of DINAME 2017*. DINAME 2017. Lectures Notes in Mechanical Engineering. Springer, Cham, pp. 215-235.

9. RESPONSIBILITY NOTICE

The authors are the only responsible for the printed material included in this paper.